IEEE Access
Multidisciplinary | Rapid Review | Open Access Journal

Received June 3, 2021, accepted June 19, 2021, date of publication July 1, 2021, date of current version July 20, 2021.

Digital Object Identifier 10.1109/ACCESS.2021.3094060

Design and Experiment of an Anthropomorphic Robot Hand for Variable Grasping Stiffness

HYEONJUN PARK[1], MYUNGHYUN KIM[1], BUMJOO LEE[2], AND DONGHAN KIM[1]
[1]Department of Electrical Engineering (Age Service-Tech), Kyung Hee University, Seoul 17104, Republic of Korea
[2]Department of Electrical Engineering, Myongji University, Seoul 17058, Republic of Korea

Corresponding author: Donghan Kim (donghani@khu.ac.kr)

This work was supported in part by the Ministry of Trade, Industry and Energy (MOTIE), South Korea, under Industrial Technology Innovation Program under Grant 20004315 and Grant 20015440, and in part by the BK21 Plus Program through the National Research Foundation (NRF) by the Ministry of Education of Korea under Grant 5120200313836.

ABSTRACT This paper introduces an anthropomorphic robot hand that has variable grasping stiffness to unknown objects without damage. The robot hand has four fingers, 13 DoFs (Degrees of Freedom) with three SEA (Series Elastic Actuator) modules in the index, middle, and ring finger. The performance for broader grasping stiffness using variable impedance control based on the parameter update block and the procedure of grasping capability evaluations of the robot hand are explained. The robot finger modules are constructed with a thumb, index, middle, and ring finger to complete the anthropomorphic type robot hand. The robot finger module has three DoFs and functions as one actuator based on an under-actuated mechanism. Additionally, external force measurement is possible in the fingertip force sensor and SEA (Series Elastic Actuator) module. For the variable impedance control implementation, a parameter update block is added to adjust the desired impedance parameter. To implement the parameter update block, we define and evaluate the correlation equation between the fingertip force, shore hardness, and damping ratio.

INDEX TERMS Anthropomorphic robot hand, modularized robot finger, multi-finger robot hand, variable grasping stiffness, impedance control, series elastic actuator module.

I. INTRODUCTION

The grasping stiffness is a parameter that must be adjusted to avoid damage when the robot hand grasps an unknown object. Humans detect elasticity with the skin and grasp objects with proper grasping stiffness [1]. Most of the research on robot hands is based on grasp taxonomy [2] proposed by Cutkosky in 1989. However, it does not consider the grasping stiffness of the robot hand, passively regulate it, or rely on the material's ductility that constitutes the robot hand. To grasp various unknown objects without damage, the grasping stiffness should be actively controlled.

For the manipulator to perform the tasks, the end-effector should be installed at the distal part to enable interaction with the object. Most end-effectors currently in use in the industry are classified into two broad categories according to task: mechanical grippers and vacuum grippers. In particular, mechanical grippers such as those shown in figure 1 are used in 2-finger type and 3-finger type grippers [3], [4]. However, these grippers are limited to transporting simple forms of objects, which is a pick-and-place.

The associate editor coordinating the review of this manuscript and approving it for publication was Bidyadhar Subudhi.

A. ANTHROPOMORPHIC ROBOT HAND

Recently, the anthropomorphic type of robot hands that can grasp and interact with various objects have been studied [5], [10]. The anthropomorphic type robot hand is a form that mimics a human hand, and it is a multi-finger type with 4-fingers or more (shown in figure 2). It is more capable of broader applications than the simple gripper type end-effector. In the last five years, most studies about the anthropomorphic robot hand have been designed with an under-actuated mechanism.

Santina *et al.* [5] deal with the complexity-dexterity trade-off by proposing a novel framework for the design of tendon driven under-actuated hands. According to the authors, the SoftHand 2 can manipulate objects of different shapes with just two DoA (Degrees of Actuator) and requires only a very simple control strategy. However, there is no feedback system for the external environment and it cannot force control. You *et al.* [7] proposed the anthropomorphic robot

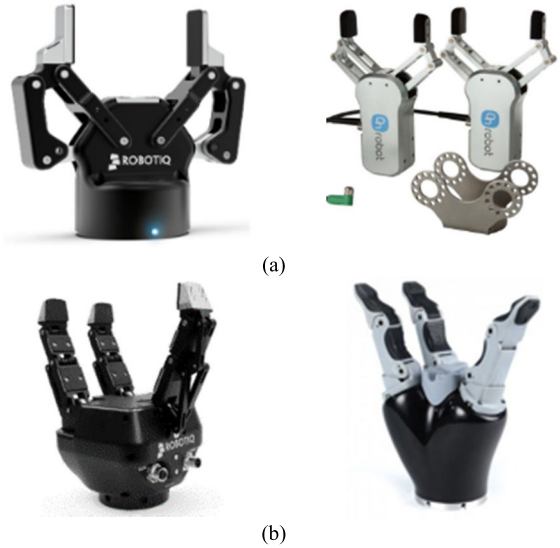

FIGURE 1. Fingered end-effectors: (a) 2-finger type, (b) 3-finger type [3], [4].

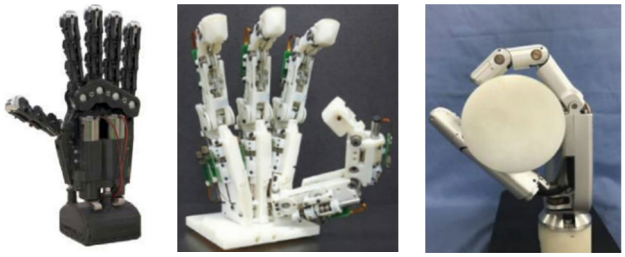

FIGURE 2. Various anthropomorphic type robot hand/finger [5]–[10].

hand with a backdrivable mechanism, an ADP (active distal-proximal) joint, and IMC (intermetacarpal) joints. This robot hand is developed to have a closer dexterity to the precision grip of the human hand without any complex control algorithm. For the evaluated the developed robot hand, they are using their own gripping strategy: the coordinate center of the workspace intersection volume of the robot fingers is used as the gripping point. Cheng *et al.* [8] proposed a high-level integrated under-actuated anthropomorphic finger with three joints and two DoF (Degree of Freedom). Moreover, this finger led to the design of a novel coupled-adaptive mechanism, and it has a multi-channel tactile sensor, angle sensor for the force and position feedback. Yoon and Choi [9] presented an under-actuated finger mechanism for implementing three DoFs motion with only one linear actuator and two springs. The aim of this research is to design a robotic finger able to perform not only natural motion but also self-adaptive grasping. Kim *et al.* [11] proposed the FLLEX Finger, a 3-DoF (Degree of Freedom) finger mechanism that is cable-driven with unique VEC pulleys, which allow high fingertip force and accurate kinematic modeling. As all the moving parts are submerged in lubrication fluid with a latex skin, the finger mechanism has high efficiency and control performance. Mańkowski *et al.* [12] developed the PUT-Hand, the five-finger anthropomorphic gripper intended for elastic object manipulation. PUT-Hand is a hybrid design, taking advantage of both fully actuated and under-actuated designs. This robot hand is equipped with tri-axial force sensors mounted on the fingertips of fully actuated fingers (index, middle, and thumb).

B. VARIABLE GRASPING STIFFNESS OF THE ROBOT HAND

The studies introduced in this part about the variable grasping stiffness of robot hands (gripper) are a method of manually controlling the grasping stiffness by transmitting the information of the object (mass, size, material, etc.) to the robot hand. Alternatively, the body of the robot hand (gripper) is composed of soft materials to minimize damage to the grasping object and control the grasping stiffness [13]–[18]. These established methods show that if the robot hand (gripper) controls the grasping stiffness, various objects can be grasped without damage. However, there is a limitation of manually controlling grasping stiffness.

Nagase *et al.* [13] developed the pneumatic robot hand with variable-stiffness fingers that can change their softness and friction. This robot hand consists of silicone rubber, fiber reinforcement, and the joint part. The softness and friction coefficient of the proposed finger can be changed by adjusting the input air pressure to the variable-stiffness finger devices. Abeach *et al.* [14] designed and tested a variable stiffness, three-fingered soft gripper. The gripper uses pneumatic muscles that are soft and inherently compliant. The stiffness of the gripper can be increased by raising the pressure in all the actuators that compose the pneumatic muscles, without the position of the fingers changing. Li *et al.* [16] present a novel structure-controlled variable stiffness robotic gripper that enables adaptive gripping of soft and rigid objects with a wide range of compliance. However, before grasp execution, the desired grasping force and the object size should be defined or pre-measured since the gripper is open loop controlled without using any force sensors at the gripper tips. Mahboubi *et al.* [17] introduced a mechanism that provides a driving force for tendon-driven hands to control the position and stiffness of the fingers with two servo motors. However, the grasping stiffness is manually controlled by the desired spring compression. Sun *et al.* [18] designed and fabricated a soft gripper with variable stiffness contributed by a pangolin inspired structure and an enhanced pneumatic actuator, and the grasping stiffness is controlled by air pressure.

The aim of this study is to develop an anthropomorphic robot hand that has variable grasping stiffness (not manually controlled) to unknown objects. This robot finger integrates the force sensor, a piezo-resistor style sensor. Our conclusion is that the proposed robot hand can detect the object's elasticity when grasping an object and react to adjust the grasping stiffness. To do this, we applied the variable impedance control using a parameter update (the detailed description written in Section III). We also demonstrate the robot hand's ability to adjust the grasping stiffness by detecting elasticity of the object using sensors of the robot finger, and the basic

ability of the robot hand (grasping force, fingertip force, and flexion/extension velocity etc.).

The paper is organized as follows. We explain the mechanical/electrical hardware of the developed robot hand and analyze the kinematics to understand the correlation of the workspace with respect to the joint space in Section II. Section III describes the controller that actuates the robot hand. The impedance controller is constructed using feedback from the fingertip force sensor and the series elastic actuator module sensor for the grasping stiffness. The proposed robot hand performance is tested through several experiments in Section IV. The conclusion is provided in section V.

II. DESIGN OF THE ROBOT HAND HARDWARE

Based on the kinematics configuration of the human hand [19]–[21], this section introduces the anthropomorphic robot hand design. The fingers, except the thumb, were composed of four links and three joints [22]–[24]. Based on the kinematic configuration, the robot finger is designed to be modularized. The robot finger modules are constructed with a thumb, index, middle, and ring finger to complete the anthropomorphic type robot hand.

A. DESIGN OF THE MODULARIZED ROBOT FINGER

The DP (Distal Phalanx), MP (Middle Phalanx), PP (Proximal Phalanx), and metacarpals of human fingers are linked, as shown in figure 3, and they are connected to DIP (Distal Inter-phalangeal), PIP (Proximal Interphalangeal), and MCP (Metacarpal) joints.

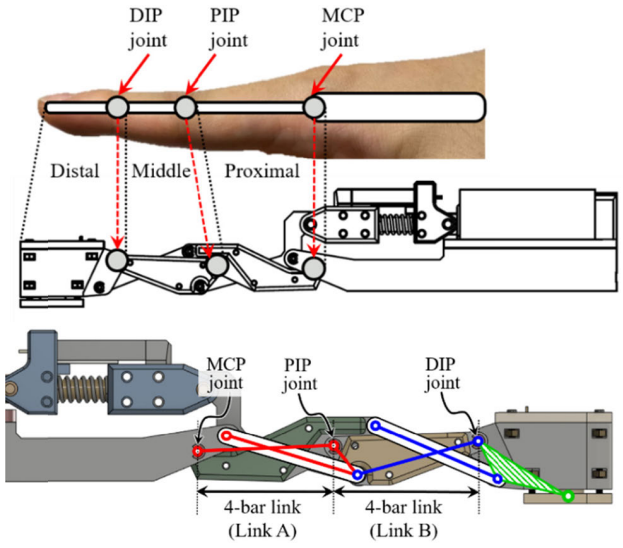

FIGURE 3. Kinematic configuration of the human finger and designed robot finger.

The purpose of this paper is to implement three DoFs as one actuator based on an under-actuated mechanism. The robot finger is determined based on the linkage mechanism with less transfer force loss of the actuator than those that are tendon-driven. Two four-bar linkages are connected in series, as shown in figure 4, so that the robot finger moves according to the actuator movement. The four-bar is the most straightforward movable closed-chain linkage. It consists of four links connected in a loop by four joints [25]. Link A corresponds to the MP in the human finger, and Link B corresponds to the PP. The actuator uses a PQ12-P linear actuator (Autonix Co., Canada), and the actuator shaft moves forward/backward according to the control signal. This actuator has a potentiometer for feedback of the actuator shaft position. The robot finger has sensors which are force sensors and a SEA (Series Elastic Actuator). As shown in figure 4 (a), the DP body has a force sensor to measure the fingertip force. The force sensor is a FSG15N1A (Honeywell Co., USA), and is detected by the piezo-resistor style. The SEA (Series Elastic Actuator) module developed in the actuator shaft (motor output) is connected. The SEA can calculate external force using Hooke's law by measuring the length of the spring. To this end, the linear potentiometer is fixed to the SEA body to measure the length of the spring. The specifications of the finger module and sensors are shown in table 1.

TABLE 1. Specifications of the robot finger and sensor part.

	Parameter	Specification
[a]Modularized robot finger	Weight	71g
	Size (length × width)	166.13 mm × 16 mm
	Fingertip force (max.)	5.3 N
	Finger speed (max.)	52.44 °/s
Force sensor (FSG15N1A)	Sensitivity	0.24 mV/gf
	Force range	0 ~ 1500 gf
	Allow over force	5500 gf
Spring	loaded length	6.1 mm
	Unloaded length	10 mm
	Stiffness (k)	5 N/mm
Linear actuator	Gear ratio	100:1
	Stall torque	50 N
	Rated voltage	12 V

[a]The specification of fingertip force and finger speed are result of experiment shown in Section IV-A.

B. KINEMATICS OF THE ROBOT FINGER

The robot finger changes the position and orientation of each link at the joint. Kinematic analysis is required to predict the position and orientation of the link with the movement of the joint. The robot finger module analyzes kinematics based on vector analysis, as shown in figure 5. In this kinematics analysis, the variable vectors are q, r_n, and p_n, and the constant vectors are a_n and b_n. The vector q is an input element of the robot finger, which expresses the movement of the actuator; and the vector p_n changes orientation, according to q, but the size does not change. Similarly, among the included angles of two different vectors, the variable angles are θ_n and α_n, and the constant angle is δ_n. The constant vectors a_n and b_n, and angle δ_n are fixed values determined in the design, and r_n is an adjusting vector for vector analysis. $\Delta\, O_1O_4A$ is an actuator

TABLE 2. Specifications of the designed anthropomorphic robot hand.

Parameter	Specification
Weight	440 g
Size (length × width)	192.18 mm × 81 mm
[a]Grasping force (average)	35.7 N

[a]The specification of grasping is result of experiment shown in Section IV.

body fixed to the metacarpals and vectors a_1 and p_1 are an actuator dimension offset. The vector p_2 is a part of the SEA module, and its size changes by an external force. However, since the kinematics analysis in this chapter proceeds in the no-load state, the size of vector p_2 is fixed. $\Delta\ O_2O_3O_4$ is the metacarpals, $\Delta\ BO_3E$ is a rocker of Link A, $\Delta\ O_2CD$ is the MP body, $\Delta\ DEF$ is the PP body, vector p_{13} is a rocker of Link B, and finally FGH is the DP body. The point O_3 is the MCP joint, point D is the PIP joint, point F is the DIP joint, and point H is the contact point of the fingertip. The MCP, PIP, and DIP joints exist only in the flexion/extension axis so that kinematics can be interpreted in the $x-y$ plane. As such, the change in the position and orientation of point H (vector p_e) according to the MCP, PIP, and DIP joints can be calculated by kinematics. The forward kinematics of the finger can be calculated as follows:

$$p_e = p_{16} + p_{11} + p_8 + b_2 \tag{1}$$

The variation of MCP, PIP, and the DIP joint by q is calculated as follows; θ_m, θ_p, and θ_d respectively represent the angle of the MCP, PIP, and DIP joints.

$$\theta_m = \pi - (\theta_1 + \delta_3 + \delta_4) \tag{2}$$
$$\theta_p = \alpha_9 + \delta_{10} \tag{3}$$
$$\theta_d = \alpha_{17} + \delta_{12} + \delta_{13} \tag{4}$$

The robot finger module RoM (Range of Motion) simulation result is shown in figure 6, based on the kinematics analysis in (1) – (4).

C. ROBOT HAND HARDWARE

The designed robot hand is shown in figure 7. The main board contains a microprocessor, a low-pass filter circuit, a Bluetooth module, and a battery. The Hand palm board has the motor driver modules, the actuator connectors, and variable sensor connectors. The fingertip boards have amplifiers for the force sensors and force sensor's connectors. The detailed specifications of the robot hand are shown in table 2. The size of the robot hand is similar to an adult men's (age 20-60) average hand size [26] (193.04 mm). Additionally, the detailed experiment of grasping force in shown in Section IV.

III. VARIABLE GRASPING STIFFNESS CONTROL

A. CONTROL ARCHITECTURE

The overall control architecture of the robot hand is shown in figure 8. The MCU (micro controller unit) is A/D (analog to digital) converting various sensor signals (actuator encoder, force sensor, SEA module sensor) to control the robot hand. The sensor signal is used as a feedback factor, and the designed controller operates the actuator. Further, the MCU communicates with a PC based on Bluetooth wireless communication. The total control cycle is 500 Hz, and the main clock of the MCU is set to 168 MHz.

TABLE 3. Result of the experiment for define parameter update block.

Parameter	Shore hardness	Range of ζ	ζ_d	Peak force
Object 1	2	$0.88 \le \zeta \le 0.91$	0.90	1.43 N
Object 2	24	$0.78 \le \zeta \le 0.83$	0.81	2.06 N
Object 3	55	$0.72 \le \zeta \le 0.78$	0.75	2.11 N
Object 4	74	$0.70 \le \zeta \le 0.73$	0.72	2.32 N
Object 5	100	$0.67 \le \zeta \le 0.71$	0.69	2.45 N

TABLE 4. List of 21 objects used in the grasping experiments.

Parameter	Shore hardness	ζ_d	ζ
Object E-1	100	0.70	0.70
Object E-2	55	0.74	0.75
Object E-3	24	0.82	0.81
Object E-4	16	0.85	0.84
Object E-5	5	0.89	0.88
Object E-6	2	0.90	0.90

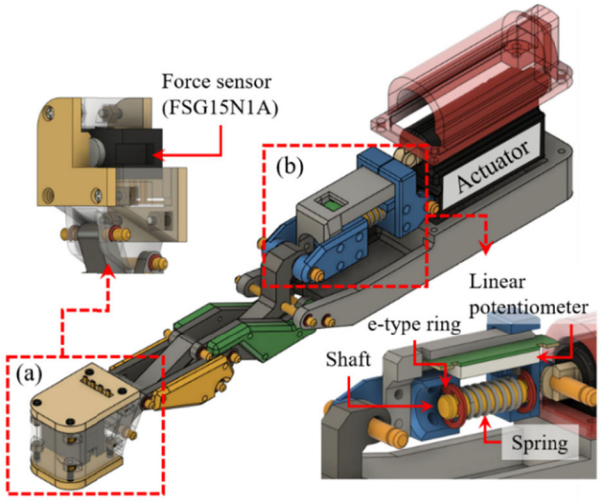

FIGURE 4. The design of the anthropomorphic robot finger module using SEA. (a) force sensor (b) SEA module.

B. VARIABLE IMPEDANCE CONTROL

Impedance control focuses on controlling the correlation between external force and motion, rather than handling position control and force control as separate problems. Applying impedance control to the robot fingers achieves the same effect as the fingertip points connected to the virtual compliance frame origin with a mass-spring-damper [27]. When the robot hand grasps the object, it should be able to determine the elasticity of the object according to the contact force. Previous studies quantified the flexibility of objects based

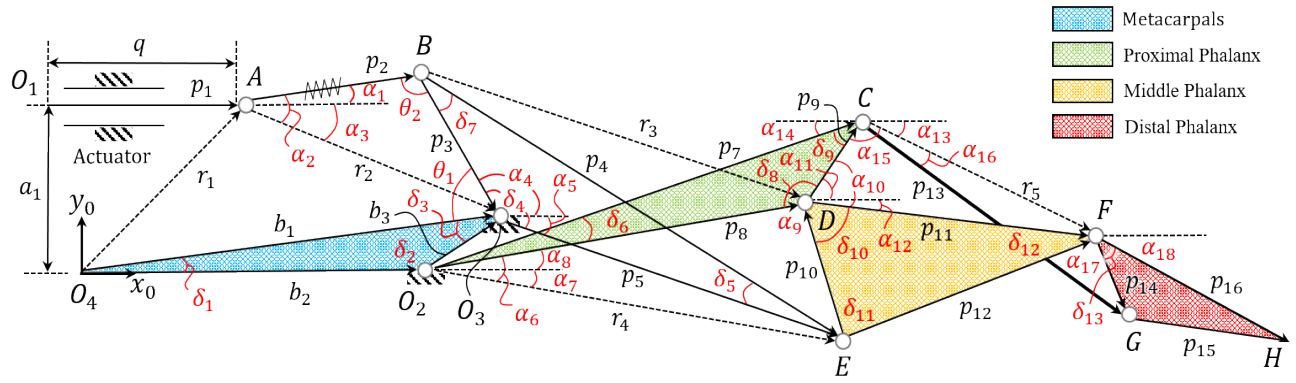

FIGURE 5. The resolution of vector for kinematics analysis.

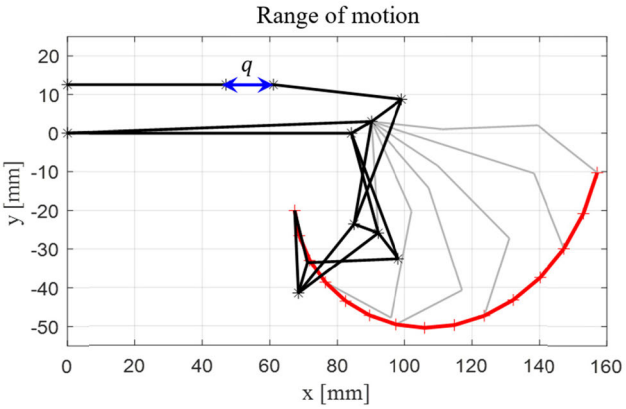

FIGURE 6. The RoM of the anthropomorphic robot finger module.

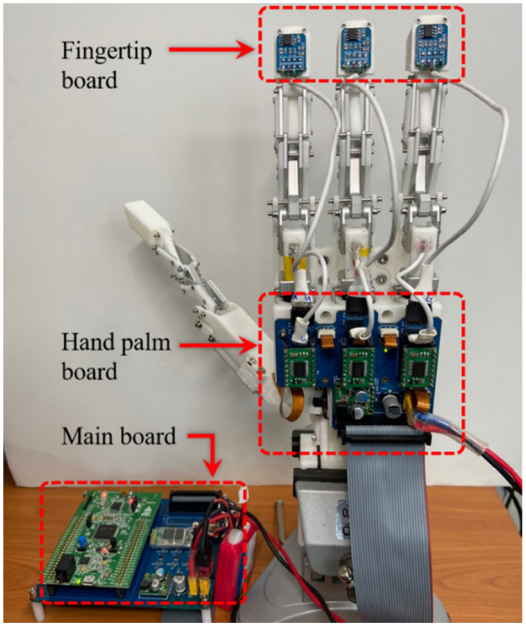

FIGURE 7. Developed anthropomorphic robot hand.

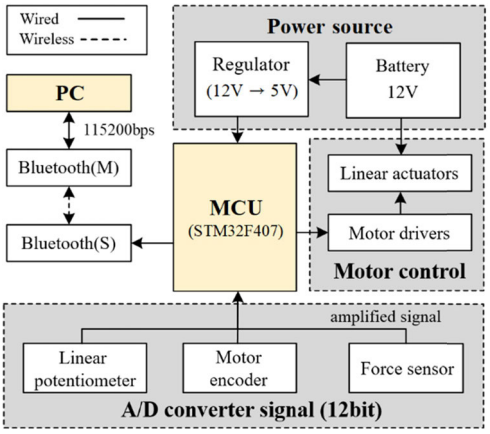

FIGURE 8. Control architecture of the robot hand.

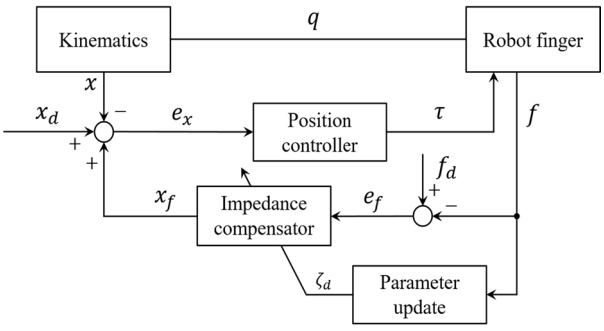

FIGURE 9. The block diagram of the variable impedance controller.

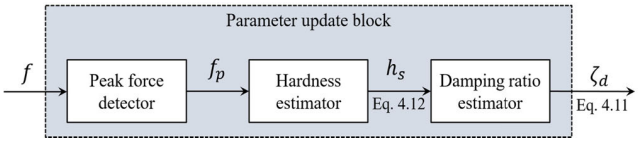

FIGURE 10. Detail flowchart of the parameter update block.

on the Shore hardness scale [28]–[32]. The Shore hardness scale is written as "50 Sh SRIS," which means the higher the number, the harder the object and the lower the number, the softer the object. When the output power of the robot finger is the same, the external force detected at the fingertips is changed by the hardness of the object. Therefore, the relationship between the Shore hardness and the external

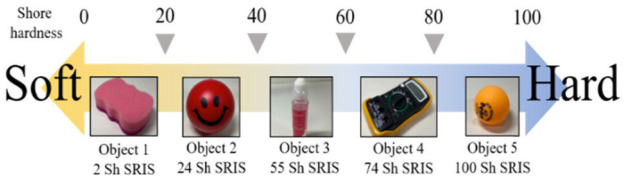

FIGURE 11. Object list for define parameter update block.

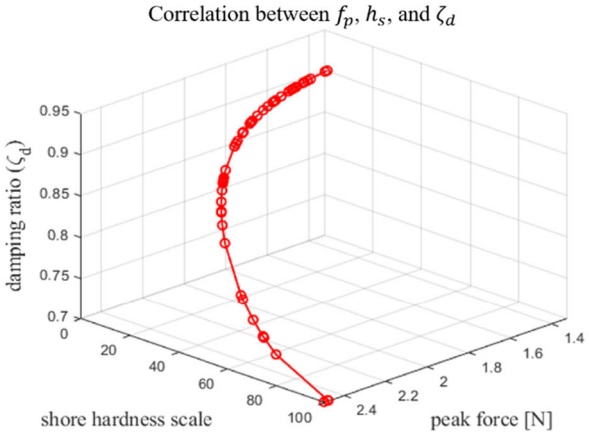

FIGURE 12. Result of the correlation between f_p, h_s, and ζ_d.

force (f) detected in the robot finger should be defined, and the parameter of desired impedance should be adjusted based on the Shore hardness. In this paper, the parameter update block, which can adjust the desired impedance parameter, is added to the general impedance controller shown in figure 9.

The parameters of the desired impedance are the damping ratio (ζ) and natural frequency (ω_n). There are several studies that apply variable impedance control by manipulating the parameters of the desired impedance [33]–[39]. In some cases, the variable impedance control is implemented by controlling the virtual damping ratio, [33], [34], and the parameter using the damping ratio is handled with a fuzzy algorithm and adjusted [35], [36]. There are cases where the pattern of the damping ratio is defined, and the experimental results are discussed for each situation [37]. To control the stiffness parameter, some cases are implemented by reflecting the damping ratio [38]. There are also cases where the variable admittance control is implemented by changing the damping parameter of the controller based on the rate of change of the force [39]. Therefore, in this paper, the parameter update block is implemented with a focus on the damping ratio. The detailed flow chart of the parameter update block is shown in figure 10. When the robot hand grasps the object, the peak value is detected in the measured force. The Shore hardness is estimated based on the peak force value, and the damping ratio is calculated from the estimated Shore hardness. In the Laplace domain, the position error $e_x(s)$ modified by the

$$x_f(s) = Z_d(s)\, e_f(s) = -\frac{f_d(s) - f(s)}{M_d s^2 + B_d s + K_d} \tag{5}$$

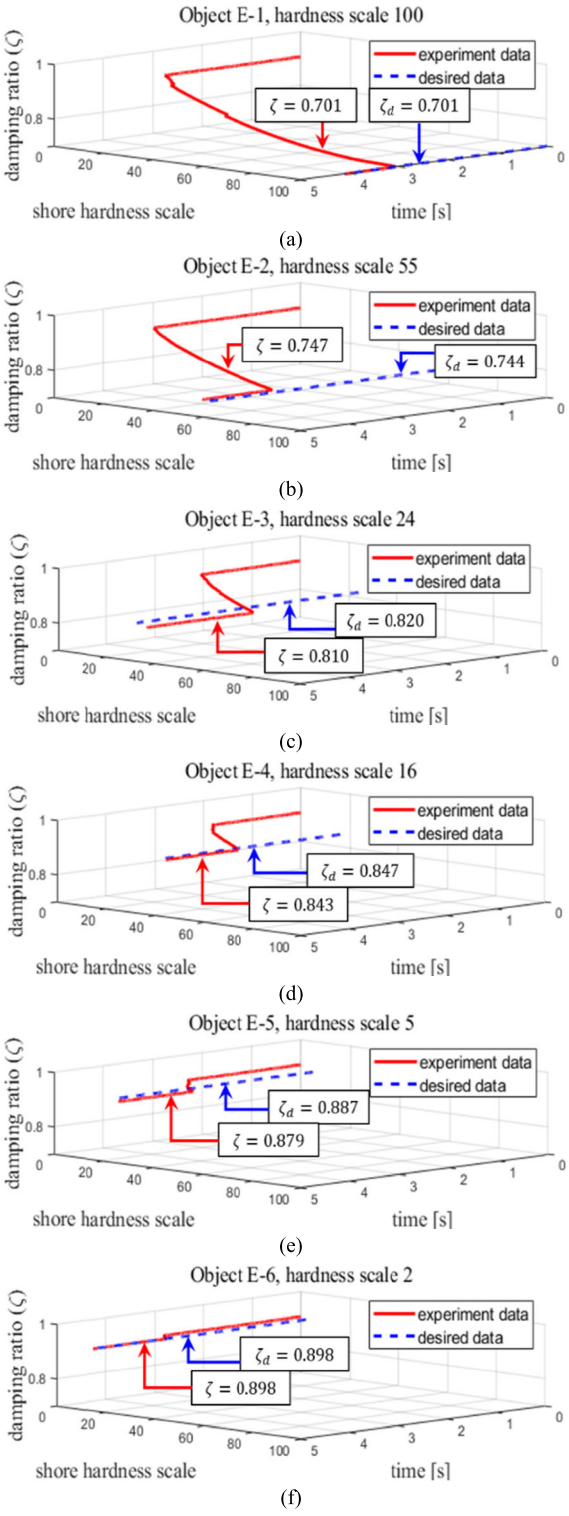

FIGURE 13. Results of the experiment about the variable impedance controller (a) object E-1 (b) object E-2 (c) object E-3 (d) object E-4 (e) object E-5 (f) object E-6.

$$e_x(s) = \left\{x_d(s) + x_f(s)\right\} - x(s) \tag{6}$$

impedance compensator, and the position compensation $x_f(s)$ are defined as (5) – (6), where $x(s)$ is the current

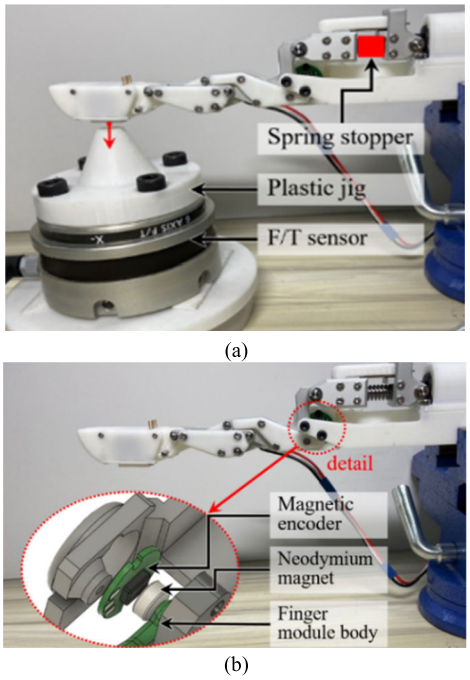

FIGURE 14. Robot finger module experiment environment. (a) fingertip force (b) finger speed.

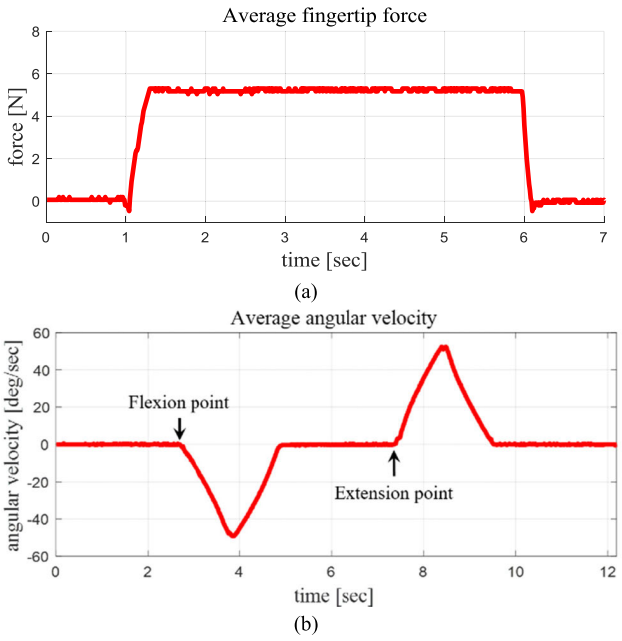

FIGURE 15. Result of the robot finger module experiment. (a) fingertip force (b) finger speed.

position, $f(s)$ is the force sensor, $f_s(s)$ is the SEA module sensor, f_d (s) is the desired force, and x_d (s) is the desired position.

First, we define the relationship between the Shore hardness and the damping ratio. The precondition for expression of a relation is when an object is grasped, slip does not occur, and the object's weight and size are not considered. For this purpose, the range of stable grasping is searched

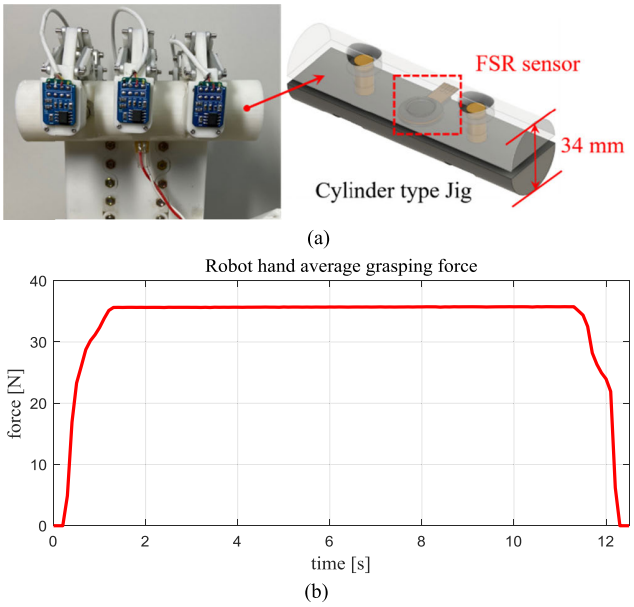

FIGURE 16. The experiment of the robot hand grasping force. (a) experiment environment (b) results of the robot hand grasping force experiment.

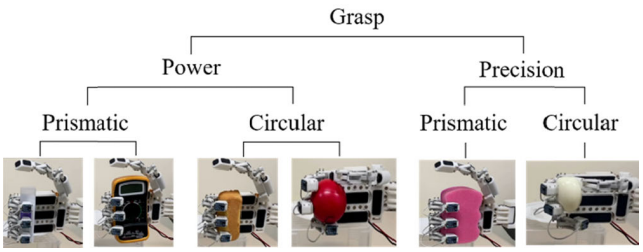

FIGURE 17. Grasping method based on the grasping taxonomy [39].

FIGURE 18. Objects set used in the grasping evaluation experiments.

using a trial and error method based on the selected object, as shown in figure 11. As a result, if ζ is smaller than 0.45,

it is impossible to grasp the object stably due to excessive vibration, and if ζ is larger than 1.25, the robot finger's has insufficient output, making it impossible to grasp stably. Therefore, the search range is set up as $0.45 \leq \zeta \leq 1.25$. The grasping experiment is carried out for each object within the set range. The data obtained from the experiments are shown in table 3. The range of ζ for each object is the range of fast settling time after analyzing the response characteristics of the robot finger position. The ζ_d is set to a median value in the range of the estimated ζ. Additionally, the peak force means the maximum force at the moment when each object is grasped.

The correlation between the Shore hardness and ζ_d is defined as (7), where h_s is a Shore hardness and α_i is a coefficient of each term. The correlation of h_s and ζ_d of (7) is a quadratic curve fitting based on the least-squares regression ($R^2 = 0.998$ of (7)). When the robot hand grasps the object, it should be able to determine the Shore hardness of the object with the value of the measured force sensor. Thus, when grasping objects 1 – 5, the correlation between the detected peak force and the Shore hardness is defined as (8). The correlation of h_s and f_p of (8) is an exponential curve fitting based on the least-squares regression ($R^2 = 0.997$ of (8)), where f_p is a peak force and β_i is a coefficient of each term (where, $0 \leq h_s \leq 100$). The final correlations of f_p, h_S, and ζ_d are shown in figure 12. After assuming the fingertip contact point as an impedance model to grasp an object, it is used after classifying the tendency through repeated experiments. Therefore, rather than directly estimating the impedance, a method of estimating the tendency and using it for the control parameter is proposed. In this chapter, the experiments conducted to define the correlation between $f_p - h_S - \zeta_d$ were all obtained through more than twenty repeated experiments, and (7) – (8) were determined based on the average values.

$$\zeta_d = \alpha_1 h_s^2 - \alpha_2 h_s + \alpha_3 \tag{7}$$

$$h_S = \beta_1 e^{\beta_2 f_p} \tag{8}$$

C. EVALUATION OF VARIABLE IMPEDANCE CONTROL

The variable impedance controller, in which the damping ratio is controlled due to the parameter update block, is verified.

The experiment is based on six objects, and each character is shown in table 4. The durometer measures the Shore hardness in table 4, ζ_d is estimated based on (7), and the ζ is experiment data from the proposed the robot hand system. The results of the experiment are shown in figure 13. The red line is the data obtained from the experiment, and the blue dashed line represents the desired data of objects used in the experiment. As a result, there is an error between ζ_d and ζ (in figure 13 (b) – (e). The maximum error is 0.006, but the effect on the controller is minimal, so the goal of this paper can be implemented.

TABLE 5. The object list used in evaluation of the variable impedance control.

No.	Label	Hardness	Grasping	L×H×W [mm]
1	Triangle glue	100	power-prismatic	32×106×32
2	Ping-pong ball	100	power-prehensile	40×40×40
3	AA battery	100	precision-prismatic	50×14×14
4	Credit card	100	power-prehensile	54×1×85
5	1 cent euro coin	100	power-prehensile	16×2×16
6	USB stick	96	precision-prismatic	42×7×17
7	Board marker	100	power-prismatic	18×124×18
8	Multimeter	74	power-prismatic	74×143×35
9	Gel pad	19	precision-prismatic	55×17×78
10	Makeup puff	5	precision-circular	50×20×50
11	Water glue	55	precision-prismatic	21×131×21
12	Large scourer	5	power-prismatic	146×87×31
13	Medium scourer	2	power-prismatic	106×67×32
14	Corner guard	16	precision-prismatic	57×24×57
15	Sponge ball	24	power-circular	60×60×60
16	Grape	49	precision-circular	30×20× 30
17	Tangerine	24	power-circular	50×38×50
18	Tangerine piece	3	precision-prismatic	32×14×18
19	Tofu	1	precision-prismatic	30×21×31
20	Boiled egg	2	precision-circular	38×45×38
21	Financier cake	5	power-prismatic	105×36×42

IV. GRASPING EVALUATION EXPERIMENTS

Before the grasping evaluation experiments, it is necessary to quantify the performance of the robot hand. Mechanical specifications (finger/hand size, spring parameter etc.,

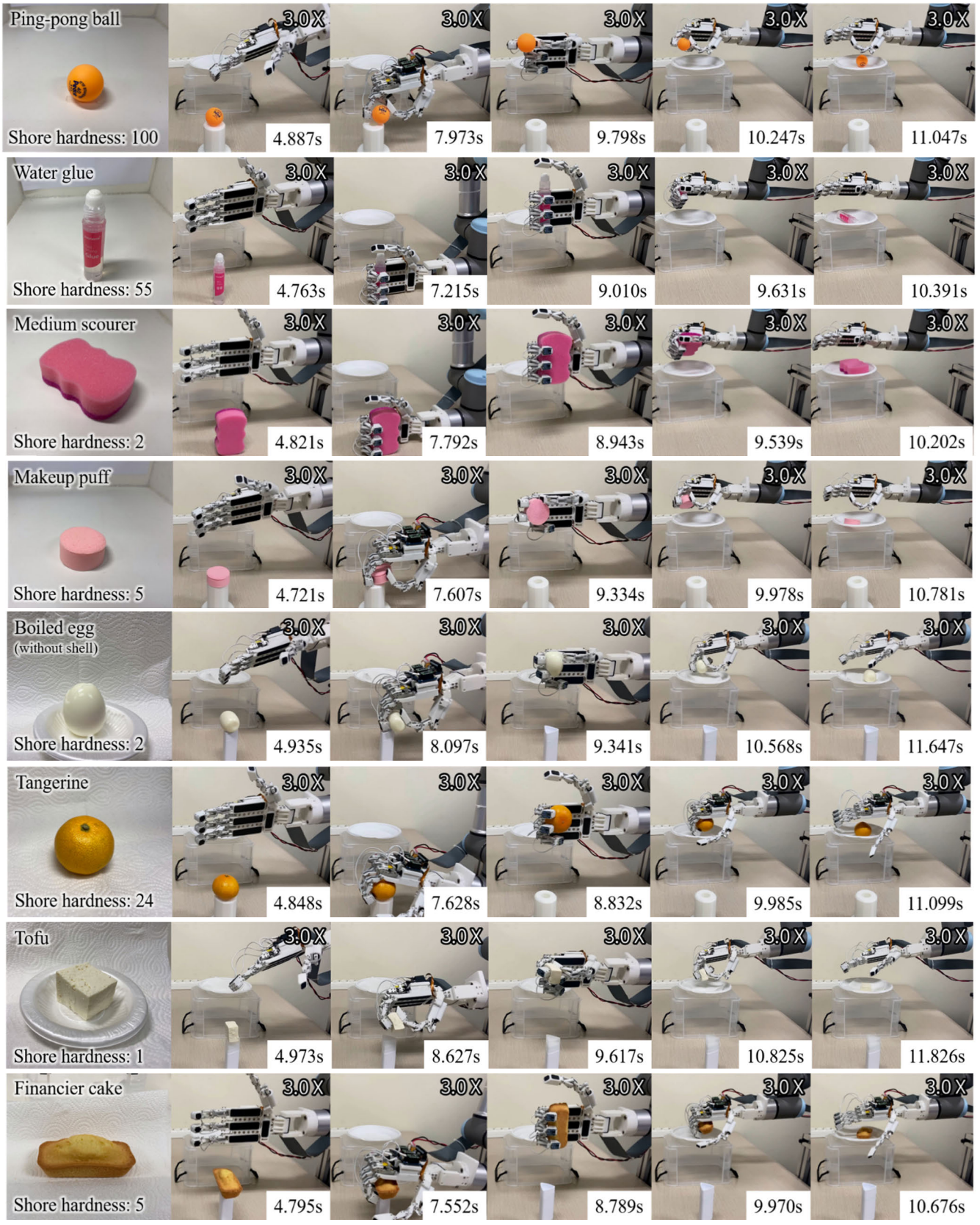

FIGURE 19. Grasping evaluation experiment video-captured images of the eight selected objects.

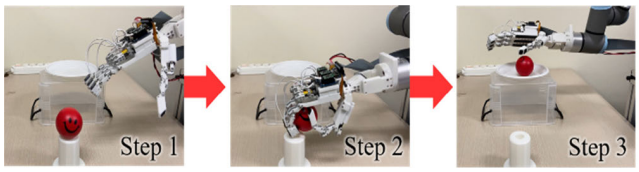

FIGURE 20. Steps of the pick-and-place task for the grasping evaluation experiment.

as indicated in tables 1 – 2) do not require an experiment for quantification. However, in the case of fingertip force, grasping force, and finger speed, experiments for quantification are needed.

A. EXPERIMENT FOR ROBOT HAND SPECIFICATIONS

The fingertip force and finger speed of the robot finger module are measured in an environment shown in figure 14. The fingertip force is measured by using the F/T (force/torque) sensor (HEX-70-XE-200N, Optoforce Co., Denmark), as shown in figure 14 (a). At his time, the movement of the SEA module is fixed to the spring stopper; the robot finger is not compressed due to the external force. The jig is developed for measuring finger speed, as shown in figure 14 (b).

The PIP and DIP joints are dependent on the MCP joints, thus measuring the angular velocity of the MCP joints. The MCP joint angle is measured from the magnetic encoder (EzEncoder, i2A Systems Co., South Korea). The measured angle is differentiated according to time to calculate the angular velocity. The results of each experiment are shown in figure 15. The maximum average force of the fingertip is 5.3 N, and the average finger speed is 52.44°/s.

To measure the grasping force of the robot hand based on the robot finger module, we made the cylinder type jig shown in figure 16. This jig has an FSR sensor built in to measure the grasping force of the robot hand. The measurement results are shown in figure 17, and the maximum average force is 35.7 N.

B. EXPERIMENT FOR ROBOT HAND GRASPING EVALUATION

The grasping method of objects used in the experiment is selected based on Cutkosky's grasping taxonomy [2]. Therefore, power grasp (prehensile –prismatic – circular) and precision grasp (circular – prismatic) should be implemented as an

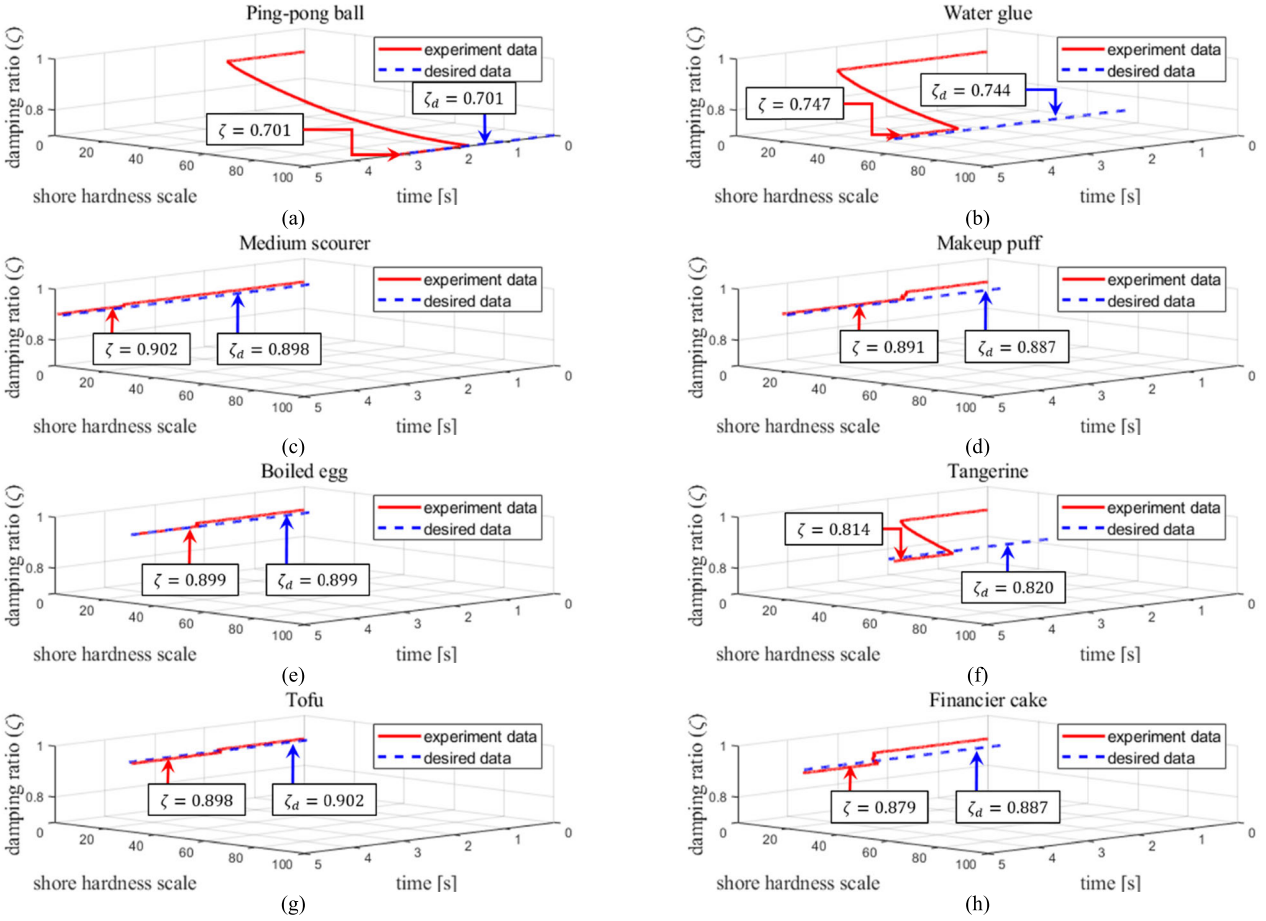

FIGURE 21. Results of the grasping evaluation experiment about damping ratio and hardness according to time of the selected eight objects. (a) Ping-pong ball (b) water glue (c) medium scourer (d) makeup puff (e) boiled egg (f) tangerine (g) tofu and (g) financier cake.

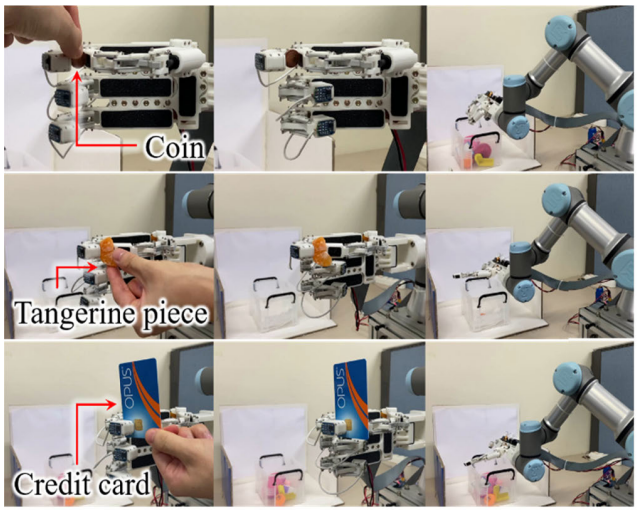

FIGURE 22. Hand-over task images of the selected three objects.

object used in everyday life to verify the performance of the developed robot hand (in figure 17). The grasping method is changed by control commands from the PC to the MCU using wireless communication. To quantify, the hardness of the object used in the experiment should be measured; therefore, the hardness of each object is measured and classified. The hardness is a measure of the resistance to localized plastic deformation induced by either mechanical indentation or abrasion. To measure hardness we used a Shore durometer (Teclock Co., Japan).

The grasping evaluation was examined by using 21 objects of various size, weight, and hardness. The classification and the characteristics of objects used in experiments are shown in figure 18 and table 5. When the robot hand grasps the object, if it is in the food group, it is easy to identify damage to the object with the naked eye. Therefore, the No. 16 – 21 objects are selected as the food group. The experiments perform pick-and-place tasks with the robot hand mounted on the manipulator (UR3, Universal Robot Co., Denmark), as shown in figure 20 (on page 9).

Figure 19 (on page 10) shows selected video-captured images of this task for eight different objects, and figure 21 (on page 11) shows the results of the evaluation experiment about damping ratio and hardness value according to time of the selected eight objects. The experimental results show that the proposed robot hand grasps each object without damage and completes the given task, and when the robot hand grasps the object, the damping ratio and the shore hardness value change according to time. This means that the parameter update block for the impedance controller operates without any abnormality based on the detection of the object's flexibility by a force sensor. However, small experimental objects, such as the USB stick, AA battery, coin, tangerine piece, and credit card, could not be grasped. In particular, the object was flat on the surface of the table, so the robot hand could not get a grip. On the other hand, when a person delivers an object to a robot hand, such as the hand-over task in figure 22, it is easy to grasp. This is possible because the task environment is adjusted so that a person can directly grasp the robot hand. The developed robot hands have these limitations.

V. CONCLUSION

In this article, we developed an anthropomorphic robot hand using a series elastic actuator module, which has variable grasping stiffness to handle unknown objects without damage. To do this, first we studied the skeleton structure of human fingers to design an anthropomorphic robot finger. Based on the kinematic configuration, the robot fingers, except the thumb, were composed of four links and three joints [19]–[24]. Second, we explain the mechanical/electrical hardware of the developed robot hand and analyze the kinematics to understand the correlation of the workspace with respect to the joint space. The purpose of this paper is to implement three DoFs as one actuator based on an under-actuated mechanism. The robot finger is determined based on the linkage mechanism. The SEA (Series Elastic Actuator) module developed in the actuator shaft is connected. Also, for detecting the external force of the fingertips, we used a force sensor. The robot finger module analyzes kinematics based on vector analysis. And the variation of the MCP, PIP, and the DIP joints by q has been calculated. The robot hand consists of four fingers (index, middle, ring, and thumb). It is sized similar to an adult male hand. Third, we describe the controller that actuates the robot hand. The total control cycle is 500 Hz, and the main clock of the MCU is set to 168 MHz. The parameter update block, which can adjust the parameters of the desired impedance, is added to the general impedance controller. The parameter update block adjusts the parameters of the desired impedance based on the Shore hardness scale [28]–[32]. The parameters of the desired impedance are the damping ratio and the natural frequency. In this paper, the parameter update block is implemented with a focus on the damping ratio by referring to studies about variable impedance control [33]–[39]. Therefore, the correlation between the detected peak fingertip force, Shore hardness, and desired damping ratio values was defined. Finally, we verified the experiment for the specifications of the robot hand and the grasping capability by performing various experiments.

For further works, the grasping experiment conducted in this study is not an optimal grasp test for the target object because it is conducted without a separate recognition algorithm, and the three fingers of the robot hand, except the thumb, can only move via flexion/extension. For more diverse movements, it is necessary to repair the adduction/abduction motion. Therefore, further studies on the optimal grasping of objects that robot hands are trying to grasp should be conducted, and the DoF of robot hands should be increased for more diverse movements. Based on this, further research needs to be done to enable in-hand manipulation.

REFERENCES

[1] I. Kao, M. R. Cutkosky, and R. S. Johansson, "Robotic stiffness control and calibration as applied to human grasping tasks," *IEEE Trans. Robot. Autom.*, vol. 13, no. 4, pp. 557–566, Aug. 1997.

[2] M. R. Cutkosky, "On grasp choice, grasp models, and the design of hands for manufacturing tasks," *IEEE Trans. Robot. Autom.*, vol. 5, no. 3, pp. 269–279, Jun. 1989.

[3] L. Birglen and T. Schlicht, "A statistical review of industrial robotic grippers," *Robot. Comput.-Integr. Manuf.*, vol. 49, pp. 88–97, Feb. 2018.

[4] (2018). *Products: Gripper, Camera and Force Torque Sensors*. Robotiq Co. Accessed: Dec. 20, 2020. [Online]. Available: https://robotiq.com/products

[5] C. D. Santina, C. Piazza, G. Grioli, M. G. Catalano, and A. Bicchi, "Toward dexterous manipulation with augmented adaptive synergies: The Pisa/IIT SoftHand 2," *IEEE Trans. Robot.*, vol. 34, no. 5, pp. 1141–1156, Oct. 2018.

[6] S. Makino, K. Kawaharazuka, A. Fujii, M. Kawamura, T. Makabe, M. Onitsuka, Y. Asano, K. Okada, K. Kawasaki, and M. Inaba, "Five-fingered hand with wide range of thumb using combination of machined springs and variable stiffness joints," in *Proc. IEEE/RSJ Int. Conf. Intell. Robots Syst. (IROS)*, Oct. 2018, pp. 4562–4567.

[7] W. S. You, Y. H. Lee, H. S. Oh, G. Kang, and H. R. Choi, "Design of a 3D-printable, robust anthropomorphic robot hand including inter-metacarpal joints," *Intell. Service Robot.*, vol. 12, no. 1, pp. 1–16, Jan. 2019.

[8] M. Cheng, L. Jiang, F. Ni, S. Fan, Y. Liu, and H. Liu, "Design of a highly integrated underactuated finger towards prosthetic hand," in *Proc. IEEE Int. Conf. Adv. Intell. Mechatronics (AIM)*, Jul. 2017, pp. 1035–1040.

[9] D. Yoon and Y. Choi, "Underactuated finger mechanism using contractible slider-cranks and stackable four-bar linkages," *IEEE/ASME Trans. Mechatronics*, vol. 22, no. 5, pp. 2046–2057, Oct. 2017.

[10] T. Yoneda, D. Morihiro, and R. Ozawa, "Development of a multifingered robotic hand with the thenar grasp function," *Adv. Robot.*, vol. 34, no. 10, pp. 661–673, May 2020.

[11] Y.-J. Kim, J. Yoon, and Y.-W. Sim, "Fluid lubricated dexterous finger mechanism for human-like impact absorbing capability," *IEEE Robot. Autom. Lett.*, vol. 4, no. 4, pp. 3971–3978, Oct. 2019.

[12] T. Mańkowski, J. Tomczynski, K. Walas, and D. Belter, "PUT-hand-hybrid industrial and biomimetic gripper for elastic object manipulation," *Electronics*, vol. 9, no. 7, pp. 1–26, Jul. 2020.

[13] J.-Y. Nagase, "Design of a variable-stiffness robotic hand using pneumatic soft rubber actuators," *Smart Mater. Struct.*, vol. 20, no. 10, pp. 1–10, Aug. 2011.

[14] L. A. T. Al Abeach, S. Nefti-Meziani, and S. Davis, "Design of a variable stiffness soft dexterous gripper," *Soft Robot.*, vol. 4, no. 3, pp. 274–284, Sep. 2017.

[15] N. Tan, X. Gu, and H. Ren, "Simultaneous robot-world, sensor-tip, and kinematics calibration of an underactuated robotic hand with soft fingers," *IEEE Access*, vol. 6, pp. 22705–22715, 2018.

[16] X. Li, W. Chen, W. Lin, and K. H. Low, "A variable stiffness robotic gripper based on structure-controlled principle," *IEEE Trans. Autom. Sci. Eng.*, vol. 15, no. 3, pp. 1104–1113, Jul. 2018.

[17] S. Mahboubi, S. Davis, and S. Nefti-Meziani, "Variable stiffness robotic hand for stable grasp and flexible handling," *IEEE Access*, vol. 6, pp. 68195–68209, 2018.

[18] T. Sun, "A soft gripper with variable stiffness inspired by pangolin scales, toothed pneumatic actuator and autonomous controller," *Robot. Comput.-Integr. Manuf.*, vol. 61, no. 1, pp. 1–12, Feb. 2020.

[19] R. Put and R. Pabst, *Sobotta's Atlas and Text-book of Human Anatomy*, 14th ed. Amsterdam, The Netherlands: Elsevier, 2006.

[20] T. Raoul, T. Jean-Michel, and M. Evelyn, *Examination of the Hand and Wrist*, 2nd ed. Oxfordshire, U.K.: Taylor & Francis, 1998.

[21] S. Cobos, M. Ferre, M. A. Sanchez Uran, J. Ortego, and C. Pena, "Efficient human hand kinematics for manipulation tasks," in *Proc. IEEE/RSJ Int. Conf. Intell. Robots Syst.*, Sep. 2008, pp. 2246–2251.

[22] G. Stillfried and P. van der Smagt, "Movement model of a human hand based on magnetic resonance imaging (MRI)," in *Proc. 1st Int. Conf. Appl. Bionics Biomech. (ICABB)*, 2010, pp. 14–16.

[23] V. J. Santos and F. J. Valero-Cuevas, "Reported anatomical variability naturally leads to multimodal distributions of Denavit-Hartenberg parameters for the human thumb," *IEEE Trans. Biomed. Eng.*, vol. 53, no. 2, pp. 155–163, Feb. 2006.

[24] P. Cerveri, N. Lopomo, A. Pedotti, and G. Ferrigno, "Derivation of centers and axes of rotation for wrist and fingers in a hand kinematic model: Methods and reliability results," *Ann. Biomed. Eng.*, vol. 33, no. 3, pp. 402–412, Jan. 2005.

[25] L. R. Norton, *Kinematics & Dynamics of Machinery*. New York, NY, USA: McGraw-Hill, 2010.

[26] R. N. Crna. (Aug. 2019). *What's the Average Hand Size for Men, Women, and Children*. Healthline. Accessed: Dec. 22, 2020. [Online]. Available: https://www. healthline.com/health/average-hand-size#adults

[27] N. Hogan, "Impedance control: An approach to manipulation: Part I-theory, II-implementation, III-application," *J. Dyn. Syst., Meas., Control*, vol. 107, no. 1, pp. 1–24, Mar. 1958.

[28] H. Yamazaki, M. Nishiyama, and K. Watanabe, "A fiber-optic mechanoreceptor in a finger-shaped end effector for human-like tactile sensing," *IEEE Sensors J.*, vol. 17, no. 16, pp. 5123–5129, Aug. 2017.

[29] N. Kashiri, D. G. Caldwell, and N. Tsagarakis, "A self-adaptive variable impedance actuator based on intrinsic non-linear compliance and damping principles," in *Proc. IEEE Int. Conf. Robot. Autom. (ICRA)*, May 2017, pp. 1248–1254.

[30] P. Fiedler, R. Muhle, S. Griebel, P. Pedrosa, C. Fonseca, F. Vaz, F. Zanow, and J. Haueisen, "Contact pressure and flexibility of multipin dry EEG electrodes," *IEEE Trans. Neural Syst. Rehabil. Eng.*, vol. 26, no. 4, pp. 750–757, Apr. 2018.

[31] Y.-L. Yu and C.-C. Lan, "Design of a miniature series elastic actuator for bilateral teleoperations requiring accurate torque sensing and control," *IEEE Robot. Autom. Lett.*, vol. 4, no. 2, pp. 500–507, Apr. 2019.

[32] J. Kwon, J. Choi, S. Lee, M. Kim, Y. K. Park, D. H. Park, and N. Kim, "Modelling and manufacturing of 3D-printed, patient-specific, and anthropomorphic gastric phantoms: A pilot study," *Sci. Rep.*, vol. 10, no. 1, pp. 1–10, Nov. 2020.

[33] A. Lecours, B. Mayer-St-Onge, and C. Gosselin, "Variable admittance control of a four-degree-of-freedom intelligent assist device," in *Proc. IEEE Int. Conf. Robot. Autom.*, May 2012, pp. 3903–3908.

[34] K. Kronander and A. Billard, "Stability considerations for variable impedance control," *IEEE Trans. Robot.*, vol. 32, no. 5, pp. 1298–1305, Oct. 2016.

[35] D. Mao, W. Yang, and Z. Du, "Fuzzy variable impedance control based on stiffness identification for human-robot cooperation," in *Proc. 3rd Int. Conf. Adv. Energy*, vol. 69, Chengdu, China, 2017, pp. 1–7.

[36] L. Roveda, S. Haghshenas, M. Caimmi, N. Pedrocchi, and L. Molinari Tosatti, "Assisting operators in heavy industrial tasks: On the design of an optimized cooperative impedance fuzzy-controller with embedded safety rules," *Frontiers Robot. AI*, vol. 6, pp. 1–19, Aug. 2019.

[37] T. Hirata, "Evaluation of acceptability of steering support method using impedance control with multiple HMIs," *J. Phys., Conf. Ser.*, vol. 1532, no. 1, pp. 1–10, Jun. 2020.

[38] L. Ye, "Trajectory tracking control of 7-DOF redundant robot based on estimation of intention in physical human-robot interaction," *Sci. Prog.*, vol. 103, no. 3, pp. 1–23, Sep. 2020.

[39] J. Bae, K. Kim, J. Huh, and D. Hong, "Variable admittance control with virtual stiffness guidance for human–robot collaboration," *IEEE Access*, vol. 8, pp. 117335–117346, 2020.

HYEONJUN PARK received the B.S. degree in robotics engineering from Hoseo University, Asan, South Korea, in 2014, and the M.S. and Ph.D. degrees in electronics engineering from Kyung Hee University, Seoul, South Korea, in 2021. Since 2021, he has been with the Research and Development Center Robot Control Team, Doosan Robotics. His research interests include the areas of robot hand, collaborative robot, mobile manipulator, and human–robot interaction.

MYUNGHYUN KIM received the B.S. degree in mechanical engineering from Kyung Hee University, South Korea, in 2021, where he is currently pursuing the M.S. degree in electronic engineering. His current research interests include robotics, especially automatic control and human–robot interaction.

BUMJOO LEE received the B.S. degree in electrical engineering from Yonsei University, Seoul, South Korea, in 2002, and the M.S. and Ph.D. degrees in electrical engineering from the Korea Advanced Institute of Science and Technology (KAIST), South Korea, in 2004 and 2008, respectively. Since 2012, he has been with the Department of Electrical Engineering, Myongji University, Seoul, where he is currently an Assistant Professor. His research interests include humanoid robotics, especially motion planning and control algorithms.

DONGHAN KIM received the B.S., M.S.E., and Ph.D. degrees in electrical engineering from the Korea Advanced Institute of Science and Technology.

He was a Postdoctoral Fellow with the University of Illinois at Urbana-Champaign, in 2003. He founded the HRI Laboratory, Kyung Hee University, which performs research in human–robot interaction, service robotics, cooperative robotics, and multi-robot systems. Prior to his position at Kyung Hee University, he was in industrial and commercial hardware development as a Senior Engineer at Samsung Electronics for three years. In that experience, he developed and led numerous mobile phone projects. He has been a Professor with the Department of Electrical Engineering, Kyung Hee University, South Korea, since 2007. His current research interest includes multi-agent robot systems.

Dr. Kim serves on the Board on International Robot-Soccer Committee, Intelligent Robot Standards Forum, and Institute of Control, Robotics and Systems.